

Anisotropic magnetic properties and giant magnetocaloric effect in antiferromagnetic $RMnO_3$ crystals ($R=Dy, Tb, Ho$ and Yb)

A. Midya, S. N. Das, and P. Mandal

Saha Institute of Nuclear Physics, 1/AF Bidhannagar, Calcutta 700 064, India

S. Pandya and V. Ganesan

UGC-DAE Consortium for Scientific Research, Khandwa Road, Indore 452 001, India

We have systematically investigated the magnetic properties and magnetocaloric effect (MCE) in $RMnO_3$ ($R=Dy, Tb, Ho$ and Yb) single crystals. Above a critical value of applied field (H_c), $RMnO_3$ undergo a first-order antiferromagnetic (AFM) to ferromagnetic (FM) transition below the ordering temperature (T_N^R) of R^{3+} moment and a second-order FM to paramagnetic (PM) transition above T_N^R . Both H and T dependence of M shows that the system is highly anisotropic in the FM as well as PM states and, as a result, the magnetic entropy change (ΔS_M) is extremely sensitive to the direction of applied field and can be negative (normal MCE) or positive (inverse MCE). For hexagonal $HoMnO_3$ and $YbMnO_3$ systems, a very small inverse MCE is observed only for H parallel to c axis and it decreases with increasing H and crosses over to normal one above H_c . On the other hand, for orthorhombic $DyMnO_3$ and $TbMnO_3$, though the inverse MCE disappears above H_c along easy-axis of magnetization, it increases rapidly with H along hard-axis of magnetization for $T \ll T_N^R$. Except for $YbMnO_3$, the values of ΔS_M , relative cooling power and adiabatic temperature change along easy-axis of magnetization are quite large in the field-induced FM state for a moderate field strength. The large values of these parameters, together with negligible hysteresis, suggest that the multiferroic manganites could be potential materials for magnetic refrigeration in the low-temperature region.

PACS numbers: 75.30.Sg, 75.47.Lx, 75.30.Kz, 75.40.Cx

I. INTRODUCTION

In twenty-first century, energy efficient and environmentally friendly technology has received special attention in order to combat the global warming phenomenon and energy crisis. Refrigeration based on the magnetocaloric effect (MCE) has attracted much research interest because of its higher energy efficiency over the conventional vapor compression refrigeration and it does not use ozone-depleting chlorofluorocarbon as a refrigerant¹. Magnetocaloric effect describes the reversible change in temperature of a material under adiabatic condition produced by the magnetic entropy change ΔS_M due to the variation in applied magnetic field^{1,2}. The main aim in this field is to search for new materials, which exhibit a large MCE and are capable of operating at different temperature ranges, depending on the intended applications. Large MCE close to room temperature would be useful for domestic and several technological applications while large MCE in the low-temperature region is important for specific technological applications such as space science and liquefaction of hydrogen in fuel industry^{1,3}. The guidelines for the choice of an appropriate material are that it should have low heat capacity and exhibit a large entropy change at the ferromagnetic (FM) to paramagnetic (PM) transition or field-induced metamagnetic transition from antiferromagnetic (AFM) to FM states with a minimal hysteresis.

In colossal magnetoresistive oxides, MCE has been extensively studied due to their wide variation in the

Curie temperature (T_C) and nature of FM-PM phase transition⁴⁻⁶. On the other hand, MCE in multiferroic manganites $RMnO_3$ ($R=Tb$ to Yb) has not been investigated in details⁷⁻⁹. So far, most of the studies on these systems are concentrated on the magnetic and ferroelectric properties of Mn sublattice because their interplay has opened up a new dimension in basic research as well as technological application. The magnetic structure determination is a prerequisite for understanding the coupling between ferroelectricity and magnetism in these materials. Several neutron and resonance x-ray studies reveal that $RMnO_3$ undergo sequence of complicated magnetic phase transitions with decreasing temperature¹⁰⁻¹⁶. It has also been shown the rare-earth magnetic ordering plays a very important role in the magnetoelectric coupling¹⁷. According to the crystallographic structure, these multiferroic materials are divided into two classes. The compounds with larger rare-earth ion ($R=Tb, Dy$) crystallize in orthorhombic structure whereas hexagonal structure is more stable for smaller ionic radius of R ($R=Ho$ to Lu, Y). In orthorhombic compounds, where the magnetic frustration of Mn spin arises from competing exchange interactions, ferroelectric and magnetic orderings appear at the same temperature¹³. However, in hexagonal compounds, the magnetic frustration of Mn spin arises from the lattice geometry since the triangular lattice is frustrated for AFM first-nearest-neighbor interaction and the ferroelectric order occurs at an elevated temperature (~ 900 K) which is well above the magnetic ordering temperature (~ 80 K)¹³.

Irrespective of the magnetic and ferroelectric properties of Mn sublattice, the AFM ordering of rare-earth moments in multiferroic $RMnO_3$ occurs at a relatively low temperature ($T_N^R < 8$ K) and the magnetic structure is highly anisotropic with very weak interaction along one of the crystallographic axes. As a result, several multiferroic manganites with high total angular momentum quantum number of rare-earth ion exhibit huge increase in magnetization at a moderate field strength (~ 2 T) which is close to the expected moment of R^{3+} ion. In this work, we present the field and temperature dependence of magnetic properties of rare-earth sublattice in $RMnO_3$ ($R=\text{Dy, Tb, Ho}$ and Yb) crystals. We observe that these materials (except $R=\text{Yb}$) exhibit giant MCE and large adiabatic temperature change and RCP due to the field-induced AFM-FM transition. This opens up a possibility for another viable technological application for multiferroic manganites namely, in magnetic cooling at low temperature. Furthermore, we have shown that one can clearly differentiate orthorhombic manganites from hexagonal ones because of their distinct magnetic and magnetocaloric properties related to rare-earth ion.

II. EXPERIMENTAL TECHNIQUES AND SAMPLE PREPARATION

Polycrystalline $RMnO_3$ ($R=\text{Tb, Dy, Ho}$ and Yb) samples were prepared from stoichiometric mixture of R_2O_3 and Mn_3O_4 by solid-state reaction and the single crystals were grown from the polycrystalline rod by travelling solvent floating zone technique using an image furnace (NEC)^{8,18}. Magnetic and heat capacity measurements were carried out employing superconducting quantum interference device magnetometer (Quantum Design) and physical properties measurement system (Quantum Design). The x-ray diffraction patterns of powdered sample of single crystals reveal that these materials are single phase. The Rietveld profile refinement of diffraction patterns shows that DyMnO_3 and TbMnO_3 have orthorhombic $Pbnm$ structure whereas HoMnO_3 and YbMnO_3 exhibit hexagonal crystal structure with space group $P6_3cm$. Several magnetic parameters such as magnetization (M), susceptibility (χ) and entropy (S_M) with field parallel to easy axis ($H\parallel e$) are denoted as M_e , χ_e and S_{Me} , respectively whereas the respective parameters with field parallel to hard axis ($H\parallel h$) are denoted as M_h , χ_h and S_{Mh} for both orthorhombic and hexagonal structures.

III. RESULTS AND DISCUSSIONS

The isothermal magnetic entropy change ΔS_M can be calculated from H and T dependence of M using the Maxwell relation, $\Delta S_M(T, H) = \int_0^H \left(\frac{\partial M}{\partial T} \right)_H dH$ ^{1,2}. Since the magnetization measurements are performed at dis-

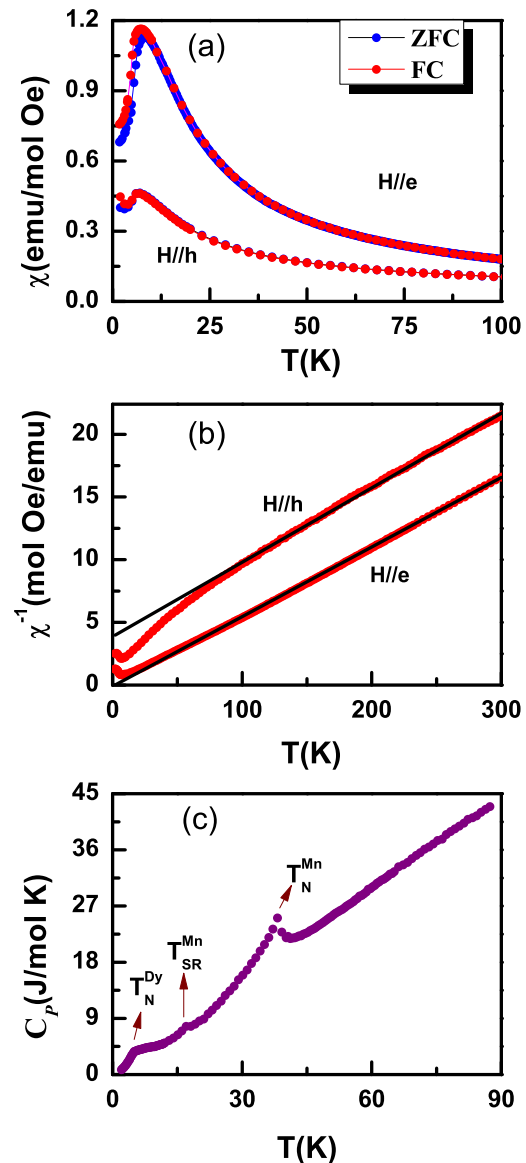


FIG. 1. (a) Temperature dependence of dc susceptibility along the easy-axis (b -axis) and hard-axis (a -axis) of DyMnO_3 . (b) Temperature dependence of χ^{-1} along both axes. Solid lines are the linear fit to the data along the respective axis. (c) Thermal evolution of heat capacity of DyMnO_3 crystal at zero field.

crete intervals of T and H , ΔS_M is numerically calculated approximately using the expression, $\Delta S_M(T, H) = \sum_i \frac{M_{i+1} - M_i}{T_{i+1} - T_i} \Delta H_i$, where M_{i+1} and M_i are the experimental values of magnetization measured with a field H_i at temperatures T_{i+1} and T_i , respectively. The characteristic parameter which determines the magnetic cooling efficiency of a magnetocaloric material is the relative cooling

power (RCP) and is defined as,

$$RCP = \int_{T_1}^{T_2} \Delta S_M dT \quad (1)$$

where T_1 and T_2 are the temperatures corresponding to both sides of the half-maximum value of ΔS_M peak. The relative cooling power is the measure of the amount of heat transfer between the cold and hot reservoirs in an ideal refrigerator as a function of field. The adiabatic temperature change (ΔT_{ad}), another important parameter related to MCE, can be calculated from the field-dependent magnetization and zero-field heat capacity data. The total entropy $S(0, T)$ in absence of magnetic field is given by

$$S(0, T) = \int_0^T \frac{C(0, T)}{T} dT \quad (2)$$

and then $S(H, T)$ may be evaluated by subtracting the corresponding ΔS_M from $S(0, T)$. The isentropic temperature change between the entropy curves $S(0, T)$ and $S(H, T)$ provides the value of $\Delta T_{ad}(T)$ ¹⁹.

A. Orthorhombic DyMnO₃ and TbMnO₃ systems

The temperature dependence of zero-field-cooled (ZFC) and field-cooled (FC) dc susceptibility χ ($=M/H$) for H ($=10$ Oe) along the easy-axis (b axis) and hard-axis (a axis) of magnetization are shown in Fig. 1(a). It is clear from the figure that DyMnO₃ is magnetically anisotropic and undergoes a PM to AFM transition below $T_N^{Dy} \sim 6.5$ K due to the long-range ordering of the Dy³⁺ moments. For further understanding the nature of magnetic interaction, we have plotted χ^{-1} versus T [Fig. 1(b)]. The linearity of $\chi^{-1}(T)$ over a wide temperature range suggests that susceptibility follows the Curie-Weiss (CW) law [$\chi=C/(T-\theta_{cw})$]. From the high temperature linear fit, we have calculated the CW temperature $\theta_{cw} \sim 2$ K and the effective moment $P_{eff} = 11.8 \mu_B$ for $H \parallel e$ while the corresponding values are -66 K and $11.6 \mu_B$ for $H \parallel h$. The observed values of P_{eff} are close to the theoretically expected moment $11.7 \mu_B$, calculated using the two-sublattice model $P_{eff} = \sqrt{(P_{eff}^{Dy})^2 + (P_{eff}^{Mn})^2}$. The large difference in θ_{cw} for two different crystallographic axes reflects the anisotropic nature of the exchange interaction. The small value of θ_{cw} indicates that the magnetic interaction along the easy axis is very weak. On the other hand, the large and negative value of θ_{cw} indicate that the magnetic interaction along the hard axis is strong and antiferromagnetic in nature. For $T \gg T_N^{Dy}$, the large difference in $\chi(T)$ between two axes implies that the system remains highly anisotropic even in the PM state. Fig. 1(c) shows the temperature dependence of specific heat in zero field. The anomalies in C_p at 38.2, 17.1 and 5.5

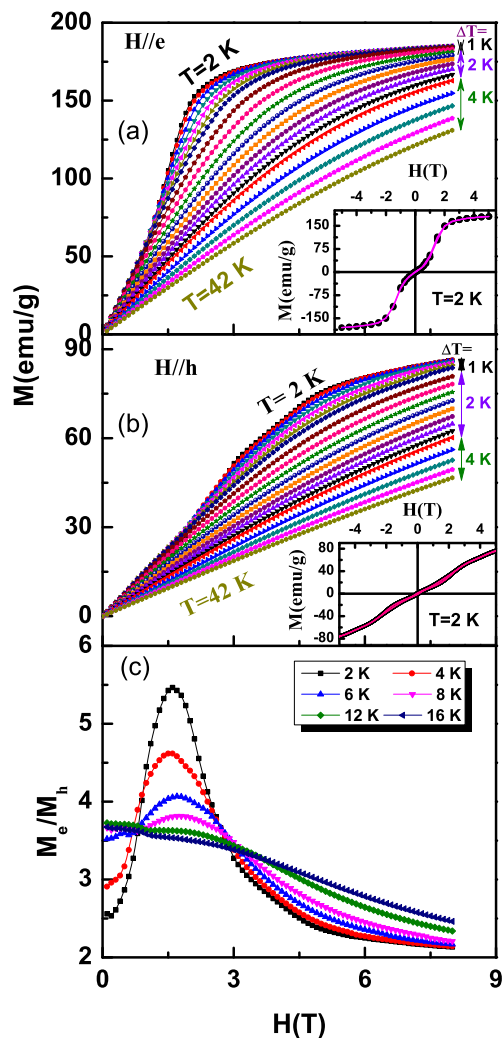


FIG. 2. Isothermal magnetization of DyMnO₃ as a function of magnetic field for different temperatures along the easy (a) and hard axes (b). Insets show the hysteresis at 2 K. Ratio of isothermal magnetization along the easy and hard axes (M_e/M_h) as a function of H at some selective temperatures (c).

K correspond to AFM transition of Mn moment (T_N^{Mn}) into a sinusoidal incommensurate phase, lock-in transition (T_{SR}^{Mn}) of Mn spin and AFM transition of Dy³⁺ ion, respectively.

For elucidating the role of applied magnetic field on AFM ordering, we have measured H dependence of M in the vicinity of T_N^{Dy} and beyond. The field is applied nearly parallel to the easy- and hard-axis of magnetization. For each isotherm, the magnetic field has been varied from 0 to 8 T. Some representative plots of isothermal field variation of M in the temperature range 2-42 K are shown in Figs. 2(a) and (b), which depict a field-induced metamagnetic transition. From these plots, one can clearly differentiate the nature of H dependence of M below T_N^{Dy} from that above T_N^{Dy} . Below T_N^{Dy} , for both

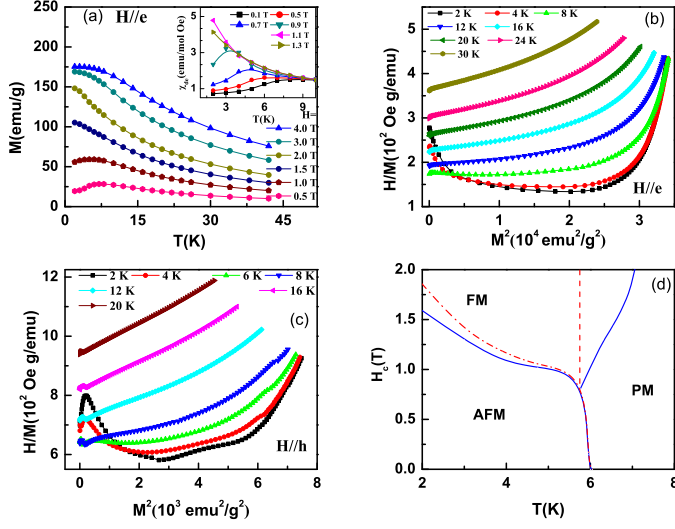


FIG. 3. (a) Temperature dependence of magnetization along the easy-axis of DyMnO₃ for different magnetic fields. Inset shows the differential susceptibility (χ_{de}) versus temperature for different fields. (b) The Arrott plots with H along the easy axis. (c) The Arrott plots with H along the hard axis. (d) The $H - T$ phase diagram of DyMnO₃.

the axes, M increases slowly with H in the low-field region followed by a sharp jump at a critical field H_c and then increases slowly with further increase of H . M does not show monotonic temperature dependence for $H < H_c$. This behavior is consistent with the field-induced transition from AFM to FM state at $H = H_c$. We observe that H_c is slightly higher and the field-induced metamagnetic transition is less sharper for $H \parallel h$ as compared to $H \parallel e$. Also, the value and nature of H dependence of M for $H \parallel h$ and $H \parallel e$ are significantly different. This is more clearly reflected in the field dependence of the ratio M_e/M_h , which shows a sharp and symmetric peak at around 1.5 T [Fig. 2(c)]. As T increases, the peak becomes broad and shifts slowly towards higher H . Above 10 K, the peak changes into a shoulder-like feature. Another important point to be mentioned here is that $M_h(H)$ curve shows a weak feature at around 5 T below T_N^{Dy} , indicating the presence of a second transition. Similar weak feature at high field has also been reported earlier in single crystals of DyMnO₃¹⁵. The insets of Figs. 2(a) and (b) display the five-segment $M(H)$ loop at 2 K. We did not observe any hysteresis at low field. This is expected because DyMnO₃ is AFM for $H < 1.5$ T. However, polycrystalline samples with small grain size may show a weak hysteresis due to the surface ferromagnetism²⁰. As the size of crystallites is quite large in good quality single crystals, the contribution from surface magnetism is very small. The value of saturation magnetization (M_s) deduced at 2 K and 8 T is $8.8 \mu_B$ for $H \parallel e$ which is 88% of expected moment ($10 \mu_B$). In contrary to this, M does not show saturation-like behavior and its value is

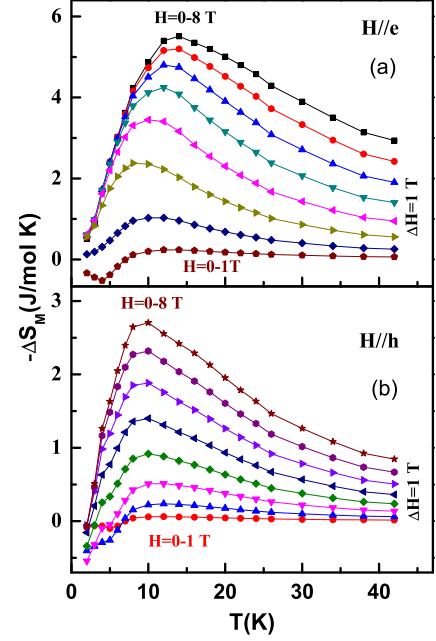


FIG. 4. Magnetic entropy change versus temperature for different field change along (a) easy axis (b) hard axis.

less than half of the expected moment for $H \parallel h$. The higher value of H_c , low magnetic moment and absence of saturation-like behavior are consistent with the large and negative value of θ_{cw} for $H \parallel h$. The temperature dependence of M and differential susceptibility χ_d ($=dM/dH$) are useful to understand the field-induced magnetic transition. Figure 3(a) shows T dependence of M and χ_d for $H \parallel e$. The peak position in $M_e(T)$ and $\chi_{de}(T)$ curves corresponds to AFM transition temperature T_N^{Dy} . T_N^{Dy} decreases rapidly with increasing H and disappears at H_c in both the cases. Above H_c , the nature of $M(T)$ curve changes dramatically. M increases rapidly with decreasing T but saturates at low temperatures. The saturation region widens with the increase of field strength. These behavior suggest that DyMnO₃ undergoes field-induced AFM-FM transition below T_N^{Dy} and PM-FM transition above T_N^{Dy} . Normally, the field-induced order-order transition is first order in nature. For understanding the nature of AFM-FM and FM-PM phase transitions, we have transformed the $M_e(H)$ data into Arrott plots as shown in Fig. 3(b)²¹. The slope of H/M versus M^2 curve is useful to determine the order of both temperature and field driven magnetic phase transition. The negative slope of the Arrott plot often indicates a first-order nature of the transition, while the positive slope implies a second-order transition²². In the present case, the negative slope below T_N^{Dy} for $H < 1.8$ T indicates that the field-induced AFM-FM transition is first-order in nature while the positive slope of the high-field data and their linear extrapolation to $H=0$ at a non-zero positive

value of M for $T_N^{Dy} \leq T \leq 20$ K suggest the second-order nature of the PM-FM transition. The Arrott plots are also done for $M_h(H)$ data [Fig. 3(c)]. Though the Arrott plots for H along two different directions are qualitatively similar below T_N^{Dy} , the nature of high-field data above T_N^{Dy} in two cases are very different. The first-order nature of AFM-FM transition is also evident from the low-field M_h data. However, the linear extrapolation of high-field M_h data to $H=0$ does not reveal any non-zero and positive value of M for $T > T_N^{Dy}$. This suggests that the PM-FM phase boundary at T_N^{Dy} is extremely sharp when the field is applied along the hard-axis of magnetization. The temperature dependence of H_c , determined from the maximum in $dM(H)/dH$ (for $T < T_N^{Dy}$) and minimum in $dM(T)/dT$ (for $T > T_N^{Dy}$) curves and the Arrott plots, is summarized in the $(H-T)$ phase diagram [Fig. 3(d)]. In order to test whether DyMnO₃ is a suitable candidate for magnetic refrigeration, we have calculated the isothermal magnetic entropy change from the $M(H)$ curves [Figs. 2(a) and (b)] using the Maxwell relation. Figure 4 presents the thermal distribution of ΔS_M for field variation up to 8 T for H parallel to easy and hard axes. In both the cases, ΔS_M is negative above T_N^{Dy} and the magnitude of $-\Delta S_M(T)$ at maximum (ΔS_M^{max}) increases with field. ΔS_M^{max} is as high as 5.52 J mol⁻¹ K⁻¹ at 8 T for $H||e$. However, the H dependence of ΔS_M below T_N^{Dy} are quite different in two cases. ΔS_{Me} is positive (inverse MCE) below T_N^{Dy} only for small field changes $\Delta H < H_c$ ($=1.5$ T). On the other hand, ΔS_{Mh} remains positive up to 8 T for $T < 3$ K. Moreover, the steep decrease in $\Delta S_{Mh}(T)$ on the low-temperature side of the maximum suggests that DyMnO₃ may exhibit a large inverse MCE below 2 K. It is worth noting that the position of the maximum in $-\Delta S_M(T)$ curve shifts slowly towards higher temperature with increasing field for $H||e$ while it is insensitive to field for $H||h$. This behavior is consistent with the observed $(H-T)$ phase diagram. For $H||e$, the positive value of ΔS_{Me} below T_N^{Dy} initially increases and then decreases with the increase of H and eventually becomes negative above 1.5 T. Such type of H dependence of ΔS_M is quite common in anti-ferromagnetic systems where the field-induced AFM-FM transition occurs¹. The initial increase in ΔS_M with H below H_c is due to the field-induced magnetic disordering. When an external magnetic field is applied along the easy axis, the magnetic moment fluctuation is enhanced in one of the two AFM sublattices which is antiparallel to H . With the increase of H , more and more spins in the antiparallel sublattice orient along the field direction. This, in turn, increases the spin disordering and it continues up to a certain field below H_c . As the system becomes ferromagnetic for $H > H_c$, the majority of spins in the antiparallel sublattice orient along the field direction and, as a consequence, ΔS_M becomes negative. The relative cooling power is evaluated to determine the cooling efficiency of DyMnO₃ crystal as a magnetocaloric material. RCP is quite large (155 J mol⁻¹) for a field change

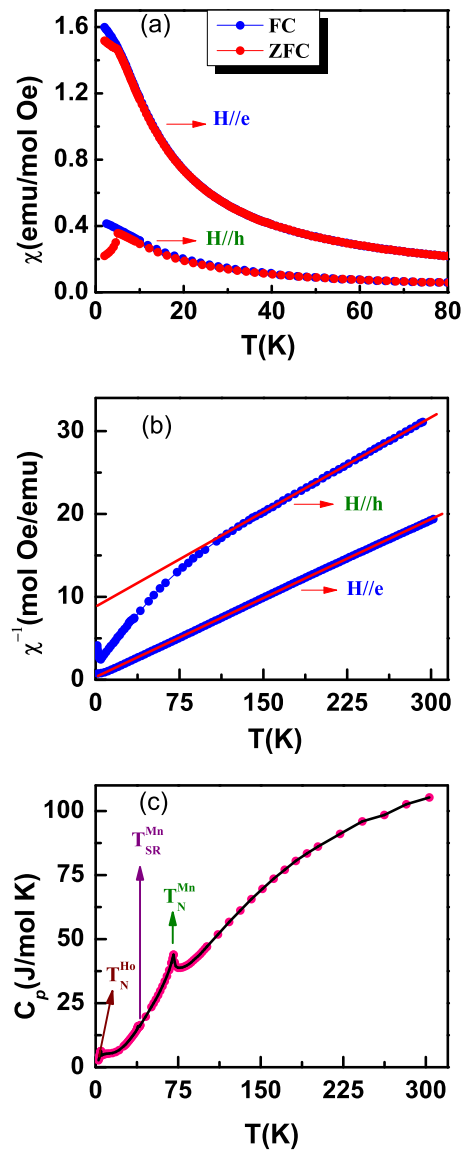


FIG. 5. (a) Temperature dependence of FC and ZFC dc susceptibility curves for HoMnO₃ along easy axis (a axis) and hard axis (c axis). (b) Inverse susceptibility versus temperature measured along easy and hard axis. Solid line indicates the Curie-Weiss fit in both directions. (c) Temperature dependence of specific heat for HoMnO₃ crystal at zero magnetic field.

of 8 T for $H||e$. We have also estimated the adiabatic temperature difference from the isentropic curves using the zero-field specific heat data in Eq. (2). ΔT_{ad} is found to be as high as 11.5 K for a field change of 8 T for $H||e$. This value of ΔT_{ad} is appreciably larger than that observed in perovskite manganites^{1,4}. Similar to DyMnO₃, the temperature and field dependence of magnetization with H along easy-axis (a axis) and hard-axis (b axis) of TbMnO₃ crystal has been measured. We observe that the T and H dependence of magnetization for TbMnO₃ crystal is similar to earlier reports⁹⁻¹¹. Unlike DyMnO₃,

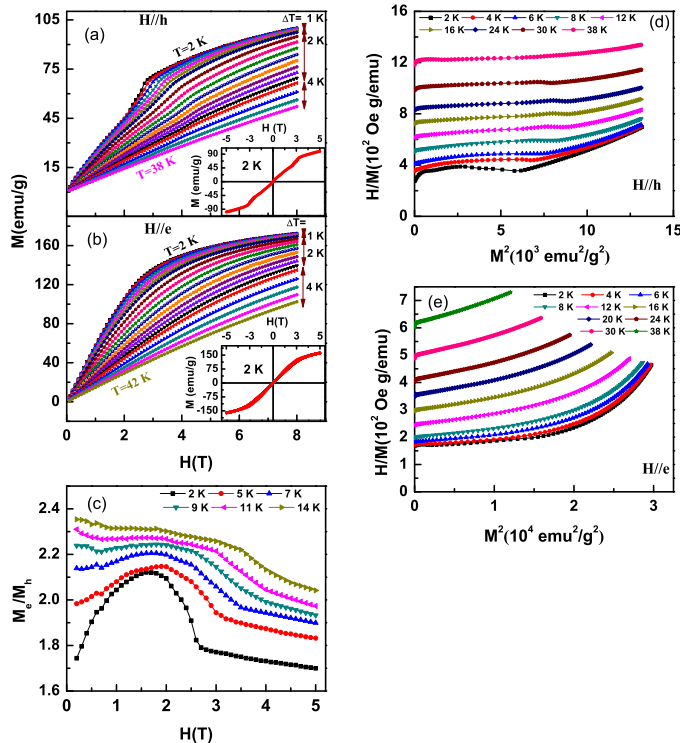


FIG. 6. Figure 6. Field dependence of isothermal magnetization for HoMnO₃ with H parallel to hard axis (a) and easy axis (b). M_e/M_h versus H plot at some selective temperatures (c). The Arrott plots of the magnetization isotherms along hard axis (d) and easy axis (e).

the inverse MCE in TbMnO₃ is appreciably large and increases with H along b axis. This suggests that the AFM ground state in TbMnO₃ is quite stable against applied field along the hard axis of magnetization. In spite of this difference, the nature of field-induced AFM-FM and PM-FM transitions and $(H-T)$ phase diagrams for $H||e$ as well as for $H||h$ are qualitatively similar in two systems. Also, we observe that the values of magnetocaloric parameters ΔS_M^{max} , RCP and ΔT_{ad} in DyMnO₃ and TbMnO₃ are comparable in magnitude. Therefore, both DyMnO₃ and TbMnO₃ satisfy the major important criteria for magnetic refrigeration at low temperatures.

B. Hexagonal HoMnO₃ and YbMnO₃ systems

The temperature dependence of low-field ($H=4$ Oe) susceptibility along the two principal axes of hexagonal unit cell of HoMnO₃ is shown in Fig. 5(a). The anomaly at 4.5 K in ZFC cycles is due to the AFM ordering of Ho moments whereas the weak bifurcation between FC and ZFC curves below ~ 40 K corresponds to the reorientation of Mn moment in the basal plane perpendicular to the initial direction. No anomaly is observed at the AFM ordering temperature of the Mn moments. Figure shows that

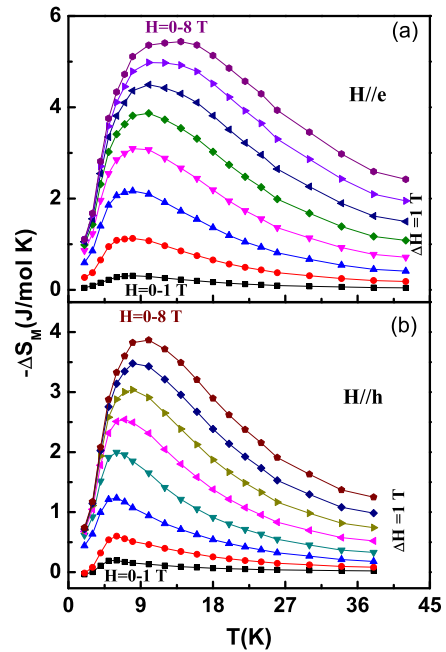


FIG. 7. Figure 7. Temperature variation of magnetic entropy change for different field change along (a) easy axis (b) hard axis for HoMnO₃.

the values of χ at any temperature are significantly different along two crystallographic directions; reflecting the anisotropic nature of the magnetic structure of HoMnO₃. For the quantitative estimation of anisotropy in magnetic parameters, we have presented $\chi^{-1}(T)$ for H along easy axis (a axis) and hard axis (c axis) [Fig. 5(b)]. Both the curves show that χ follows the CW behavior over a wide range of T . From the linear part of $\chi^{-1}(T)$ for $H||h$, the fitted values of P_{eff} and θ_{cw} are found to be $10.24 \mu_B$ and -116 K, respectively while the corresponding values are $11.2 \mu_B$ and -5 K for $H||e$ which are consistent with the previously reported results²³⁻²⁶. Significant anisotropy in magnetic interaction is evident from the large difference in the values of P_{eff} and θ_{cw} for two principal axes of the unit cell. Unlike susceptibility, the temperature variation of zero-field heat capacity is showing three distinct transitions [Fig. 5(c)]. The peak at 4.6 K indicates the AFM ordering of Ho moment as evidenced from magnetic measurement. The small peak at ~ 39 K is due to the Mn moment reorientation and the third λ -type anomaly originates from the AFM ordering of the Mn³⁺ magnetic moments. Figures 6(a) and (b) present the field dependence of isothermal magnetization for HoMnO₃ with field parallel to c and a axes, respectively. We would like to mention that M (at 3 K and 5 T) is 20-25% larger for the present sample than the reported value on HoMnO₃ single crystal grown by the flux method²⁰. The $M(H)$ isotherms for $H||h$ indicate a field-induced metamagnetic transition. At low fields, the dependence of M on H is approximately linear and the slope of $M(H)$ curve decreases

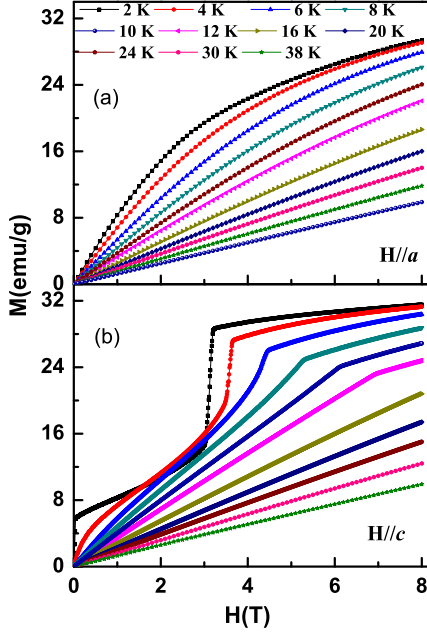


FIG. 8. Figure 8. Isothermal magnetization of YbMnO_3 as a function of magnetic field for different temperatures with H along the a axis (a) and c axis (b).

above a critical field but no saturation is attained up to 8 T. To investigate the reversibility of the field-induced magnetic transition, we have measured the five-segment $M(H)$ loop at 2 K and observed no significant hysteresis [Inset of Fig. 6(a)]. The nature of $M(H)$ curves for $H\|e$ differs from those for $H\|h$. For $H\|e$, $M(H)$ curve displays no abrupt change but increases smoothly with H and the value of M is significantly larger as compared to that for $H\|h$. The anisotropy in the field-induced FM state is apparent from the M_e/M_h versus H plot for different T [Fig. 6(c)]. The field and temperature dependence of M_e/M_h for HoMnO_3 may be compared with that for orthorhombic DyMnO_3 . One can clearly see that there are several important differences between the two systems. For example, in DyMnO_3 , the peak in M_e/M_h versus H plot is very sharp at low temperature. On the other hand, the maximum for HoMnO_3 is quite broad and its height is almost half of that for DyMnO_3 . Also, the nature of T dependence of the peak are quite different in two cases. With increasing T , though the peak broadens, the value of M_e/M_h at peak increases slowly in HoMnO_3 while the peak decreases and broadens rapidly in DyMnO_3 . Figures 6(d) and (e) show the Arrott plots for field along both the axes. The Arrott plots show that the field-induced AFM-FM transition is first order while PM-FM transition is second order and the PM-FM phase boundary is quite sharp for field along hard-axis of magnetization [Fig. 6(d)]. However, closer inspection shows that the nature of the Arrott plots for $H\|e$ [Fig. 6(e)] differs significantly from that for $H\|h$ and also from that for orthorhombic systems. For $H\|e$,

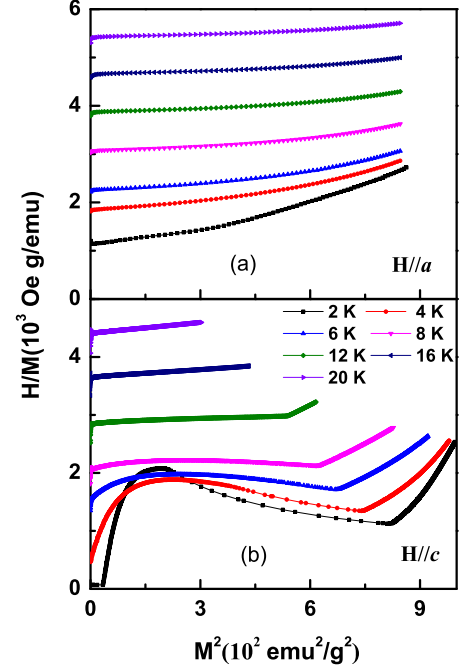


FIG. 9. Figure 9. The Arrott plots of the magnetization isotherms for YbMnO_3 with field direction parallel to a axis (a) and c axis (b).

H/M versus M^2 curves do not show negative slope in low-field region as expected for the first-order transition. This is due to the smooth increase of M with H [Fig. 6(b)]. For $H\|h$, the H/M versus M^2 curves for HoMnO_3 are almost linear in the high-field region both above and below T_N^{Ho} . Normally, the H/M versus M^2 curves are linear and parallel for mean-field like FM-PM transition otherwise an upward curvature is exhibited as in the case of $H\|e$. A small deviation from parallelism may occur due to the weak field dependence of T_C in the high-field region. Thus it appears that the system may belong to different universality class depending on the direction of applied magnetic field. For HoMnO_3 , the isothermal entropy change for different field variations was estimated. Figures 7(a) and (b) depict the nature of $\Delta S_M(T)$ curves for $H\|e$ and $H\|h$, respectively. In both the cases, a broad maximum is observed. Apart from the values, there are several important differences in the nature of H dependence of ΔS_M for two crystallographic axes. With the increase of magnetic field, the maximum in $\Delta S_M(T)$ shifts to higher temperature for $H\|e$ while the position of the maximum remains pinned at ~ 5 K for $H\|h$. For $H\|e$, ΔS_M is negative down to 2 K even at very low fields, i.e., inverse MCE is absent in the AFM state. However, for $H\|h$, ΔS_M is positive well below T_N^{Ho} at low fields ($H < H_c$). Unlike DyMnO_3 , inverse MCE in HoMnO_3 is very small. One can see that ΔS_M^{max} is large for a moderate field change along easy axis. The values of other mag-

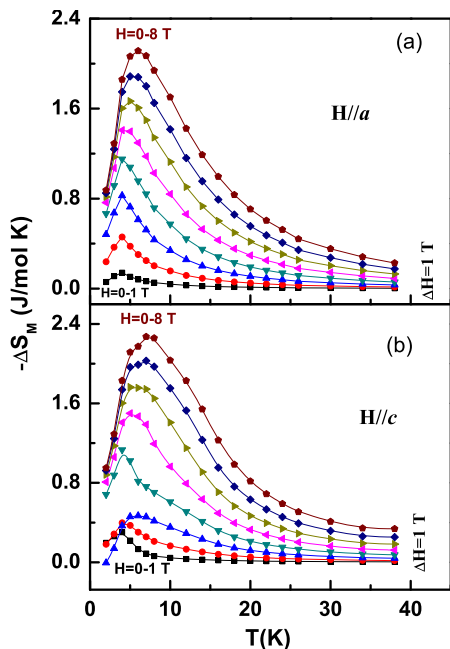


FIG. 10. The magnetic entropy change in YbMnO₃ for a field change from 0-1 to 0-8 T along the *a* axis (a) and *c* axis (b).

netocaloric parameters such as RCP and ΔT_{ad} are also large for HoMnO₃ single crystals. We observe RCP=144 J mol⁻¹ and ΔT_{ad} =12.5 K for the field change of 8 T along easy axis.

We now briefly discuss the magnetic and magneto-thermal properties of YbMnO₃ crystal. Similar to other multiferroic manganites, magnetic properties of rare-earth sublattice in YbMnO₃ is sensitive to the direction of applied field with respect to crystallographic axis. Figure 8 shows the field dependence of magnetization for YbMnO₃ at different temperatures. One can see that the nature of magnetic response of the crystal with field along *a* and *c* axes are very different. Unlike HoMnO₃, *M* is slightly larger along the *c* axis as compared to basal plane and two field-induced transitions are clearly visible. However, *M* along *a* axis increases smoothly with *H* similar to that in HoMnO₃ crystal. The transition at high-field (~ 3 T) is extremely sharp (step-like) below T_N^{Yb} ($=3.6$ K), shifts progressively towards higher field with increasing *T* and clearly visible up to 14 K [Fig. 8(b)]. It is also interesting to note that *M* does not show saturation-like behavior up to 8 T and the value *M* at 2 K and 8 T for both the axes are comparable and about 37-39% of the expected moment. This behavior is quite different from other multiferroic manganites where *M* along two axes are significantly different and the observed high-field value of *M* for *H*||*e* is close to expected moment. This suggests that YbMnO₃ is magnetically less anisotropic and the AFM interaction along both the axes is strong. Indeed from the magnetization measurements in the paramagnetic state, we observe that θ_{cw} is large and negative along both the crystallographic axes

and their values are 195 and 225 K within the basal plane and along *c* axis, respectively. In order to determine the order of field-induced magnetic transition, we have also done the Arrott plots of magnetization data of YbMnO₃ [Fig. 9]. The nature of the Arrott plots for *H* along *a* axis is qualitatively similar to those for HoMnO₃ crystal but for *H* along *c* axis the low-field peak is quite prominent and the change in slope from positive to negative is abrupt, marked by a much sharper triangular-shaped minimum at H_c . However, unlike HoMnO₃, the linear extrapolation of high-field magnetization data to $H=0$ reveals a non-zero positive value of *M* up to $2T_N^{Yb}$ for *H* along *c* axis. Figure 10 illustrates the temperature dependence of ΔS_M in a magnetic field change up to 8 T. ΔS_M reaches a negative maximum value ~ 2.3 J mol⁻¹ K⁻¹ for $\Delta H=8$ T. Though the magnitude of ΔS_M is smaller for YbMnO₃ due to the smaller total angular momentum quantum number, the overall nature of *T* and *H* depen-

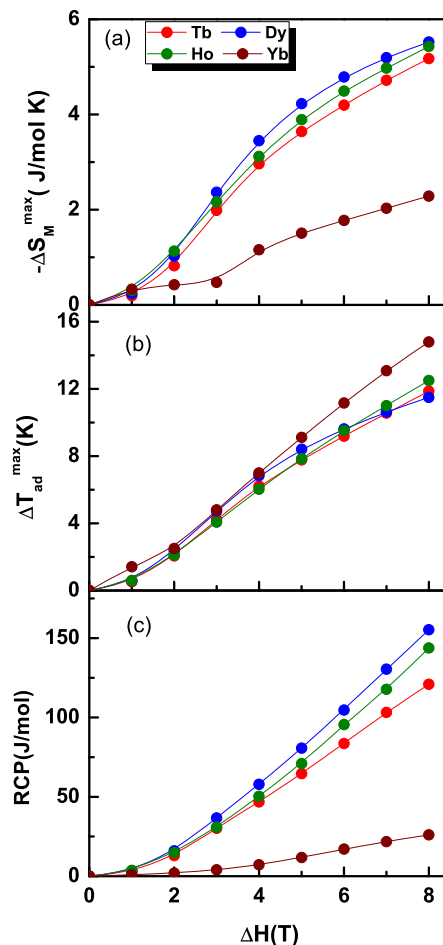


FIG. 11. The maximum of magnetic entropy change (a), maximum adiabatic temperature change (b) and relative cooling power (c) as a function of field for *RMnO*₃ crystals with *H* parallel to easy axis.

dence of ΔS_M is similar to HoMnO_3 . We observe that the value of ΔT_{ad} is significantly large (~ 15 K) in spite of its smaller ΔS_M and RCP (26 J mol^{-1}). In order to compare and contrast the nature of MCE among multiferroic manganites, the variation of ΔS_M^{max} , ΔT_{ad}^{max} and RCP for $H||e$ have been plotted in Fig. 11 which shows that these parameters increase monotonically with ΔH . Though the values of ΔS_M^{max} , ΔT_{ad}^{max} and RCP depend on the system, the nature of their field dependence is qualitatively similar. It is clear from the figures that among the four systems we have studied, DyMnO_3 , TbMnO_3 and HoMnO_3 are most suitable as low temperature refrigerant due to the high values of magnetocaloric parameters at a moderate field change.

IV. CONCLUSIONS

In conclusion, the detailed analysis of magnetization data shows that the magnetic interaction within the rare-earth sublattice in multiferroics RMnO_3 is highly anisotropic (except $R=\text{Yb}$). Above a critical field H_c , RMnO_3 undergo a field-induced first-order metamagnetic transition from AFM to FM state and a second-order PM-FM transition along with huge magnetic entropy change. Depending on T and the direction of applied field, ΔS_M can be negative or positive, i.e., RMnO_3 exhibit both normal and inverse MCE. Except at low tem-

peratures well below T_N^R , ΔS_M is negative and large in the field-induced FM state. For orthorhombic DyMnO_3 and TbMnO_3 , the inverse MCE is small, decreases with H and eventually crosses over to normal one above H_c for $H||e$ while it is large and increases with H for $H||h$. In contrary to this, hexagonal HoMnO_3 and YbMnO_3 may show small inverse MCE only below H_c and at very low temperature for $H||c$. Both orthorhombic and hexagonal multiferroics, except YbMnO_3 , exhibit giant MCE, and large adiabatic temperature change and relative cooling power for $H||e$. The large values of these parameters, negligible hysteresis and highly insulating nature suggest that the multiferroic manganites could be potential materials for magnetic refrigeration in the low-temperature region. The present results also show that orthorhombic and hexagonal multiferroic manganites can be differentiated based on the magnetic and magnetocaloric properties of rare-earth sublattice.

V. ACKNOWLEDGEMENTS

The authors would like to thank A. Pal for technical help during sample preparation and measurements. V. Ganesan would like to thank DST, India for financial assistance for the physical property measurement system facility at UGC-DAE CSR, Indore.

-
- ¹ K. A. Gschneidner Jr., V. K. Pecharsky, and A. O. Tsokol, Rep. Prog. Phys. **68**, 1479 (2005), and references therein.
- ² A. M. Tishin in *Handbook of Magnetic Materials*, edited by K. H. Buschow, (Elsevier), V-12, p. 395.
- ³ V. Provenzano, J. Li, T. King, E. Canavan, P. Shirron, M. DiPirro, and R. D. Shull, J. Magn. Magn. Mater. **266**, 185 (2003).
- ⁴ M. Phan and S. Yu, J. Magn. Magn. Mater. **308**, 325 (2007).
- ⁵ Z. B. Guo, Y. W. Du, J. S. Zhu, H. Huang, W. P. Ding, and D. Feng, Phys. Rev. Lett. **78**, 1142 (1997).
- ⁶ P. Sarkar, P. Mandal, and P. Choudhury, Appl. Phys. Lett. **92**, 182506 (2008).
- ⁷ F. W. Fabris, M. Pekala, V. Drozd, J-F. Fagnard, Ph. Vanderbemden, R. S. Liu, and M. Ausloos, J. Appl. Phys. **101**, 103904 (2007).
- ⁸ A. Midya, P. Mandal, S. Das, S. Banerjee, L. S. S. Chandra, V. Ganesan, and S. R. Barman, Appl. Phys. Lett. **96**, 142514 (2010).
- ⁹ J. L. Jin, X. Q. Zhang, G. K. Li, Z. H. Cheng, L. Zheng and Y. Lu, Phys. Rev. B **83**, 184431 (2011).
- ¹⁰ S. Quezel, F. T. Cheou, J. Rossat-Mignod, G. Quezel, and E. Roudaut, Physica B & C **86-88**, 916 (1977).
- ¹¹ T. Kimura, T. Goto, H. Shintani, K. Ishizaka, T. Arima, and Y. Tokura, Nature (London) **426**, 55 (2003); T. Kimura, G. Lawes, T. Goto, Y. Tokura, and A. P. Ramirez, Phys. Rev. B **71**, 224425 (2005).
- ¹² R. Kajimoto, H. Yoshizawa, H. Shintani, T. Kimura, and Y. Tokura, Phys. Rev. B **70**, 012401 (2004).
- ¹³ X. Fabreges, I. Mirebeau, P. Bonville, S. Petit, G. Lebras-Jasmin, A. Forget, G. Andre, and S. Pailhes, Phys. Rev. B **78**, 214422 (2008).
- ¹⁴ S. Nandi, A. Kreyssig, J. Q. Yan, M. D. Vannette, J. C. Lang, L. Tan, J. W. Kim, R. Prozorov, T. A. Lograsso, R. J. McQueeney, and A. I. Goldman, Phys. Rev. B **78**, 075118 (2008).
- ¹⁵ R. Feyerherm, E. Dudzik, A. U. B. Wolter, S. Valencia, O. Prokhnenko, A. Maljuk, S. Landsgesell, N. Aliouane, L. Bouchenoire, S. Brown, and D. N. Argyriou, Phys. Rev. B **79**, 134426 (2009).
- ¹⁶ R. Feyerherm, E. Dudzik, N. Aliouane, and D. N. Argyriou, Phys. Rev. B **73**, 180401(R) (2006).
- ¹⁷ F. Yen, C. R. de la Cruz, B. Lorenz, Y. Y. Sun, Y. Q. Wang, M. M. Gospodinov, and C. W. Chu, Phys. Rev. B **71**, 180407(R) (2005); O. Prokhnenko, R. Feyerherm, E. Dudzik, S. Landsgesell, N. Aliouane, L. C. Chapon, and D. N. Argyriou, Phys. Rev. Lett. **98**, 057206 (2007).
- ¹⁸ P. Mandal, B. Bandyopadhyay, and B. Ghosh, Phys. Rev. B **64**, 180405(R) (2001); P. Mandal and B. Ghosh, Phys. Rev. B **68**, 014422 (2003).
- ¹⁹ V. K. Pecharsky and K. A. Gschneidner Jr., Phys. Rev. Lett. **78**, 4494 (1997).
- ²⁰ E. Galstyan, B. Lorenz, K. S. Martirosyan, F. Yen, Y. Y. Sun, M. M. Gospodinov, and C. W. Chu, J. Phys.: Condens. Matter **20**, 32541 (2008).
- ²¹ A. Arrott and J. Noakes, Phys. Rev. Lett. **19**, 786 (1967).
- ²² B. K. Banerjee, Phys. Lett. **12**, 16 (1964).

- ²³ H. Sugie, N. Iwata, and K. Kohn, *J. Phys. Soc. Jpn* **71**, 1558(2002).
- ²⁴ B. Lorenz, F. Yen, M. M. Gospodinov, and C. W. Chu, *Phys. Rev. B* **71**, 014438 (2005).
- ²⁵ B. Lorenz, A. P. Litvinchuk, M. M. Gospodinov, and C. W. Chu, *Phys. Rev. Lett.* **92**, 087204 (2004).
- ²⁶ O. P. Vajk, M. Kenzelmann, J. W. Lynn, S. B. Kim, and S.-W. Cheong, *Phys. Rev. Lett.* **94**, 087601 (2005).